J Therm Anal Calorim (2012) 108:163–170
DOI 10.1007/s10973-011-1942-6

Structural characterization and thermal behaviour of biological hydroxyapatite

Anna Kohutová · Pavla Honcová · Ladislav Svoboda · Petr Bezdička · Monika Maříková

Received: 31 July 2011 / Accepted: 20 September 2011 / Published online: 11 October 2011

Abstract Thermal study and structural characterization of biological hydroxyapatite (HA) samples were done as well as their comparison with commercial and synthetic samples in this study. The X-ray micro analyser shows that all three samples of human teeth (HT1–HT3) contain two types of HA structures with different crystallite sizes, unlike sample of bovine thigh-bone (BTB). The bone sample was composed only of one HA phase with varied porosity. The molar Ca/P ratio in biological samples was lower compared to theoretical ratio for pure HA; moreover, in the case of teeth, Ca/P ratio varyies between the centre and the periphery of the cross-sectional samples. Thermogravimetry of the biological samples showed mass decreases—three regions for the bone and four regions for the teeth. In comparison, commercial HA has only two-step weight loss and synthetic HA three-step weight loss. After the calcination up to 1280 °C all the samples of teeth transformed into whitlockite, β-$(Ca,Mg)_3(PO_4)_2$ (98 wt%) and 2 wt% HA. Besides, HT3 contained further trace amount of hilgenstockite (HIL, $Ca_4P_2O_9$). The sample BTB partly transited from natural HA into HIL (6 wt%) and lime, CaO (14 wt%). X-ray powder diffraction (XRD) proved occurrence of HIL (9 wt%) beside stability part HA (91 wt%) in the commercial HA after thermal treatment but the synthetic HA composed from $Ca_3(PO_4)_2$ (74 wt%) and HA (26 wt%).

Keywords Hydroxyapatite · Hard tissues · X-ray powder diffraction · Scanning electron microscope · Thermal analysis · Mass spectrometry

Introduction

The biological hard tissues consist of apatitic structure in the form of hydroxyapatite (HA, $Ca_{10}(PO_4)_6(OH)_2$). Nevertheless, biological HA is poorly crystalline, non-stoichiometric and of submicron dimensions [1]. Besides, it contains often substitute ions: Na^+, K^+, Mg^{2+} for Ca^{2+}; CO_3^{2-} for PO_4^{3-}; HPO_4^-, F^-, Cl^-, CO_3^{2-} for OH^- and some water. This mineral phase is found in dental, enamel, dentine, and bone as well as pathological calcification (e.g. kidney stones, bile stone, dental calculus, vascular calcification, etc.). In addition, various calcium phosphates (CPs) occurred in biological human systems, for example, brushite (BRU, $CaHPO_4{\cdot}2H_2O$), tricalcium phosphate (TCP, $Ca_3(PO_4)_2$), amorphous calcium phosphate (ACP, $Ca_x(PO_4)_y$), whitlockite (WHI, β-$(Ca,Mg)_3(PO_4)_2$), fluorapatite (FA, $Ca_{10}(PO_4)_6F_2$), fluorhydroxyapatite (FHA, $Ca_{10}(F,OH)_2(PO_4)_6$) etc. [2, 3]. CPs might be added to assorted bio-applications [4, 5]. HA is widely used as surface coating of orthopaedic and dental metal implants, bio-ceramics' preparation, repair of periodontal bony

A. Kohutová (✉) · P. Honcová (✉) · L. Svoboda
Faculty of Chemical Technology, Department of Inorganic Technology, University of Pardubice, Doubravice 41, 532 10 Pardubice, Czech Republic
e-mail: an.kohutova@centrum.cz

P. Honcová
e-mail: pavla.honcova@upce.cz

P. Bezdička · M. Maříková
Institute of Inorganic Chemistry of the ASCR, v. v. i, Husinec-Řež 1001, 250 68 Řež, Czech Republic

defects, ridge augmentation, ear implants, drug carrier for controlled drug release based on adsorption/desorption properties of bioactive molecules (growth hormone, antibiotics). Moreover, technical grade CPs are very popular mineral fertilizers and they are used in catalyst [6, 7], and environmentalism for industrial- and radioactive-waste disposal [8, 9].

In biological systems, many organisms, ranging from bacteria and isolated cells to invertebrates and vertebrates, synthesize CPs [10]. The morphology of precipitates in these organisms complies with the necessities for rapid mobilization and intracellular control of the concentration of calcium and phosphorus [11]. Biological HA is not well defined for the variability in the impurities, changeability in Ca/P molar ration and solubility. Detailed information on the chemical composition of the most important human normal calcified tissues is compiled in Table 1 [12, 13]. The main constituents can vary by a percent or more.

Many kinds of HA synthesis methods, such as solid state reactions, chemical precipitation, hydrothermal reactions, sol–gel methods and mechanochemical methods have been introduced [14–17]. Variations in parameters that affect the synthesis are necessary in others to produce HA particles of desired size, crystallite, composition and specific surface area.

Analytical methods, such as electron microscopy, infrared microscopy with Fourier transformation, Raman spectroscopy, X-ray powder diffraction (XRD) and thermal analysis are generally used for qualitative and quantitative classifications of biological samples. The thermal decomposition and structural study of biological materials—urinary stones [18, 19], bones [20–22], enamel and dentin [23]—have been studied many times.

This study is concentrated on thermal analysis and structural characterization of biological HA contained in hard tissues—bovine thigh-bone (BTB) and human teeth (HT1–HT3). The results for biological samples were compared with the synthetic hydroxyapatite (sHA) and commercial hydroxyapatite (cHA).

Experimental

Hard tissues

Biological samples used in this study were obtained from patients of a private stomatological practice of the north Bohemia (human teeth: central incisor HT1, first premolar HT2, and second molar HT3). A BTB was selected as natural sample of HA. The acquired samples were cleaned using surgical alcohol to remove any blood clots, washed with distilled water, and dried at room temperature. All the samples were cut transversely into thin sections approx. 3 mm thick (Buehler Low Speed Saw, USA), which were polished to a thickness of 2 mm of cross-section. These samples were observed by the scanning electron microscope with energy dispersive X-ray spectrometer (SEM-EDX). Later, cross-sectional samples were powdered separately in an impact mill (~2 min). The powder was filtered through a 125-μm sieve and stored in a desiccator at room temperature under vacuum for subsequent analysis.

sHA and cHA

The cHA was obtained from Sigma Aldrich Steinheim (99.999%). The synthetic prepared sample (sHA) was precipitated from calcium hydroxide solution (1.85 g $Ca(OH)_2$ in 250 cm^3 distilled water) and orthophosphoric acid (1.73 g of 85% H_3PO_4 in 250 cm^3 distilled water) [13]. The acid was added to the base at a rate approximately equal to 3.5 cm^3 per min, later heated to 95 °C, and stirred for 1 h at 400 RPM. The reaction mixture was stirred for 2 h followed by cooling to room temperature and setting of precipitate overnight. Precipitate was then filtered, washed, with distilled water (three times) and dried at 60 °C in an oven.

Structural and microstructural analysis

The SEM-EDX, using JOEL JSM-5500 LV apparatus equipped with analyser IXRF Systems and detector

Table 1 The compositions and structural parameters of human calcified tissues and HA

	Matrix/wt%			Crystallite	Lattice parameters		Calcination 800 °C
	Inorganic	Organic	Water	Size/nm	*a*/Å	*c*/Å	
Enamel	97	1.5	1.5	$10^5 \times 50 \times 50$	9.441	6.880	β-TCP + HA
Dentin	70	20	10	$35 \times 25 \times 4$	9.421	6.887	β-TCP + HA
Cement	60	25	15	[a]	[a]	[a]	β-TCP + HA
Bone	65	25	10	10–30	9.410	6.890	HA + CaO
HA[b]	100	–	–	200–600[c]	9.430	6.891	HA

[a] Mostly similar to dentin

[b] Synthetic hydroxyapatite

[c] Crystallite size after calcination (800 °C)

Gresham Sirius 10, was employed to study the composition and the chemical heterogeneity of biological samples. Accelerating voltage U = 20 kV, SE signal, high vacuum mode were applied. Accuracy of EDX analysis is better than ±0.5 at.%. The existing phases in all samples were identified by X-ray diffraction (XRD) technique using PANalytical X'PertPRO with Co Kα X-ray tube (U = 40 kV, I = 30 mA) and Fe β-filter. Approximate qualitative analysis was performed using HighScore software package (PANalytical, The Netherlands, version 1.0d). Diffrac-Plus software package (Bruker AXS, Germany, version 8.0), and JCPDS PDF-2 database [24]. XRD was used to characterise all powders before every thermal treatment and after TGA-DTA measurements up to 1280 °C.

Thermal analysis

Thermal analysis was performed on Setsys Evolution 1750, TGA/DTA (Setaram). The excellent symmetry in the detectors guaranties very good baseline stability and very high detection limit for thermal measurement (sensitivity = 0.03 μg). The calorimeter was coupled to mass spectrometer QMS 403/4 (Balzers) for gas analysis. Only selected gases were analysed in regime multiple ion detection for mass: 14-F^+, 15-CH_3^+, 17-OH^+, 18-H_2O^+, 28-CO^+, 30-NO^+, 31-P^+, 38-F_2^+, 44-CO_2^+, 46-NO_2^+, 64-SO_2^+ and 142-$P_2O_5^+$. Approximately 4 mg of powdered sample, and reference substance (α-Al_2O_3, Merck) were heated (the rate 10 °C min^{-1}) in the temperature range from 25 to 1280 °C in a flowing argon atmosphere (30 cm^3 min^{-1}). Crucibles (0.1 cm^3) and thermocouples were of platinum.

Results and discussion

Human teeth

Three specimens of human teeth investigated in this study do not originate from one person. Therefore, we can expect some variation in their compositions caused by difference in teeth-owners' diets, oral care, illnesses etc. In all samples only the phase HA was observed by XRD and the space group $P6_3/m$. The quantitative estimation of individual phases using Rietweld analysis (RA) showed that all three teeth HT1–HT3 contain two types of HA structures with different crystallite sizes, the first structure (HA1) was poorly crystallised with crystallite size ~6 nm and the second one (HA2) was more crystallised than HA1 with crystallites ~35 nm. The SEM-EDX analysis was used on cross-sectional samples for indication of structural zones and colour differences, which generally correspond to variable chemical element content. Figure 1 shows the studied cross-sectional samples and selected areas for chemical element analysis marked with letters from A to F with the results summarised in Table 2. The element analysis was done from different parts of the sample to verify if there is any compositional change between the centre and periphery of studied teeth.

Figure 2 shows the thermal curves of samples HT1–HT3. The differences between weight loss and shapes of

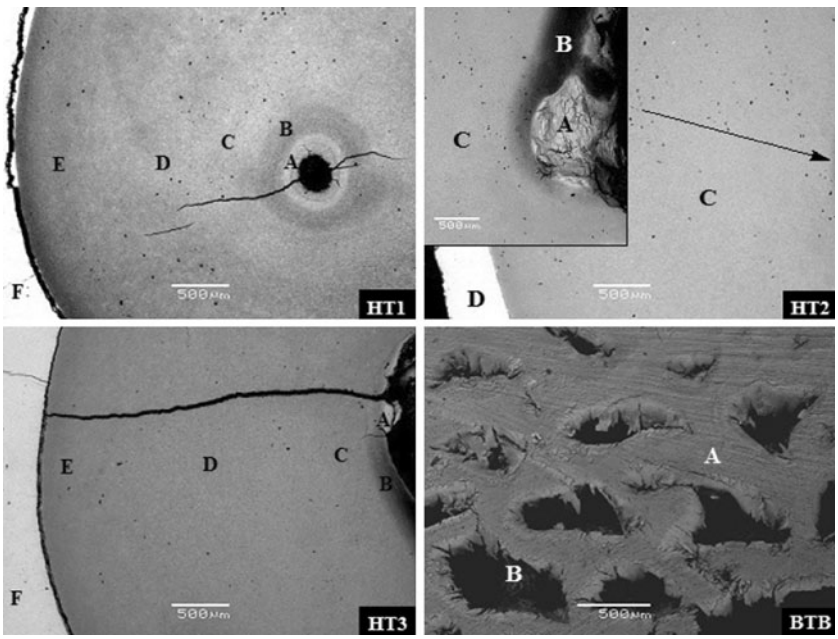

Fig. 1 Structural details of the natural samples: *HT1–HT3* human teeth and *BTB* bovine thigh-bone. *Letters* indicate areas for chemical elemental analysis

Table 2 EDX results from the cross-sectional samples of hard tissues

Sample	Zone	Compositions/at.%						Ca/P
		O	P	Ca	Na	Mg	Al	
BTB	A[a]	72.01	10.59	16.61	–	–	–	1.57
	B[a]	71.92	10.87	16.80	–	–	–	1.55
HT1	A	67.00	12.24	18.38	0.61	0.81	0.97	1.50
	B	67.40	12.14	18.12	0.69	0.91	0.75	1.49
	C	66.60	12.34	18.94	0.73	0.83	0.56	1.53
	D	66.75	12.32	18.86	0.77	0.75	0.55	1.53
	E	66.66	12.42	18.95	0.85	0.66	0.47	1.53
	F	62.21	13.99	22.35	0.73	0.21	0.51	1.60
HT2	A[b]	62.60	14.47	19.29	1.67	0.38	1.42	1.33
	B[b]	69.88	10.68	13.16	2.41	0.40	3.36	1.23
	C	66.54	12.09	17.93	1.11	0.69	1.65	1.48
	D	67.17	11.98	17.93	0.87	0.73	1.32	1.50
	E	68.26	11.74	17.53	0.79	0.57	1.11	1.49
	F	62.93	14.07	21.27	0.96	0.22	0.56	1.51
HT3	A[b]	66.46	12.19	16.37	2.26	0.33	2.25	1.34
	B[b]	67.07	10.39	11.94	2.76	0.35	7.39	1.15
	C	64.19	12.96	17.53	2.32	0.60	2.41	1.35
	D	62.57	14.08	22.34	0.86	0.24	0.54	1.59

[a] Content of zinc: 0.78 at.% (A) and 0.42 at.% (B)

[b] Trace amount of copper

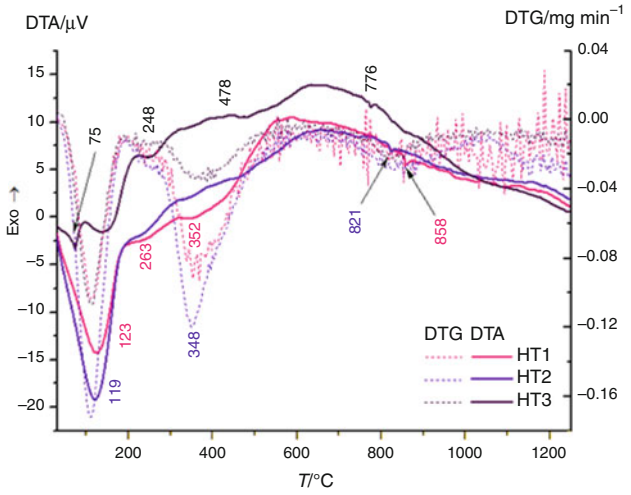

Fig. 2 DTA/DTG curves of the powdered biological samples HT1, HT2 and HT3

the curves might be attributed to the specific natural origin. The curves show four, relatively resembling regions. The first gradual weight loss about 4–6% between 30 and 200 °C, with an endothermic process, is due to liberation of the coordinated water molecule and fractional decarboxylation of samples. The process is accompanied by small amounts of release fragments F^+, OH^+, CO^+, NO^+, P^+, F_2^+, CO_2^+ or NO_2^+ (Table 3). The second step of weight loss up to ~620 °C is due to decomposition organic matrix with release of CO_x, NO_x–, SO_2^+ and the other fragments such as F^+, OH^+ and $P_2O_5^+$. This second step has comparable weight loss (about 14%) for samples HT1 and HT2, but is significantly lower (about 6%) for sample HT3. This is followed by the third step of smaller weight loss around 800 °C, caused by transformation to $Ca_3(PO_4)_2$. The last weight loss between 1000 to 1280 °C revealing almost no effect on DTA curves should be connected with the transformation into other CPs, but except HT1 sample, no fragments in escaped gases were detected (see Table 3). In the cases of HT2 and HT3, MS of the undergoing gas observed fragments F^+ and F^{2+}, which were not proved by XRD or EDX analysis. Perhaps higher concentration of fluorides collects in the centre of crystal structure of hard tissues, but the total amount of F^+, and F^{2+} ions is not enough to form FHA or FA. Effect of fluoride on the surface on dental enamel is widely used as fluoride-containing toothpaste, where the remineralization fluor—HA is related to the solubility decreasing, and it is known as way to protect teeth [25, 26].

Table 3 Thermo-analytical data and mass spectroscopy results of the samples

Sample	Loss of weight/%	Range of variation/°C	Fragments[a]
cHA	0.2	30–354	18, *44*
	1.0	354–1,280	44
sHA	0.8	30–197	18
	2.9	197–636	18, 44
	0.7	636–1,280	18, *44*
BTB	5.8	30–200	18, 28
	20.6	200–559	*15*, 18, *28*, 30, *44*, 46, 64
	15.9	559–1,280	28, 44
HT1	4.5	30–200	18, 28, 30
	14.4	200–570	18, 28, 30, 44, 46
	5.9	570–990	28, *30*, *64*
	4.3	990–1,280	28
HT2	5.6	30–190	*17*, 18, *28*, 30, 31, *44*, *46*
	13.3	190–620	*14*, *17*, 18, *28*, 30, 31, 44, *46*, *64*, *142*
	6.0	620–1,030	28, *44*
	4.3	1,030–1,280	–
HT3	3.6	30–196	*14*, 17, 18, *30*, *31*, *38*, *44*
	6.0	196–571	*17*, *18*, *28*, 30, 31, 44, *46*, *64*, *142*
	4.5	571–1,072	28, *44*
	1.4	1,072–1,280	–

[a] *14* F^+, *15* CH_3^+, *17* OH^+, *18* H_2O^+, *28* CO^+, *30* NO^+, *31* P^+, *38* F_2^+, *44* CO_2^+, *46* NO_2^+, *64* SO_2^+, *142* $P_2O_5^+$

Trace amounts are in italics

Bone

A BTB structure was studied by XRD and it shows that only HA with the space group $P6_3/m$ and crystallite size ~13 nm is presented. The SEM-EDX analysis on cross-sectional sample shows that the bone is porous and homogeneous.

The TG/DTA analysis of bone was performed in the temperature range from 25 to 1280 °C, and the obtained curves are shown in Figs. 3 and 4. Results of weight loss together with the corresponding temperature ranges and mass spectrometer analysis are given in Table 2. The TG curve of sample BTB shows larger weight loss up to 200 °C, which is caused by dehydration and decarboxylation. The second mass loss between 200 and 560 °C is as high as 20.6% of weight, and is due to the liberation of H_2O, CO_2, NO_x, SO_2 fragments and small amounts of the other fragments as e.g. CH_3^+. In this temperature range, the effect represents organic matter as protein and eventually crystalline water. The endothermic process at 1015 °C is caused by decarboxylation of organic matrix and it is accompanied by weight loss of 15.9 wt%.

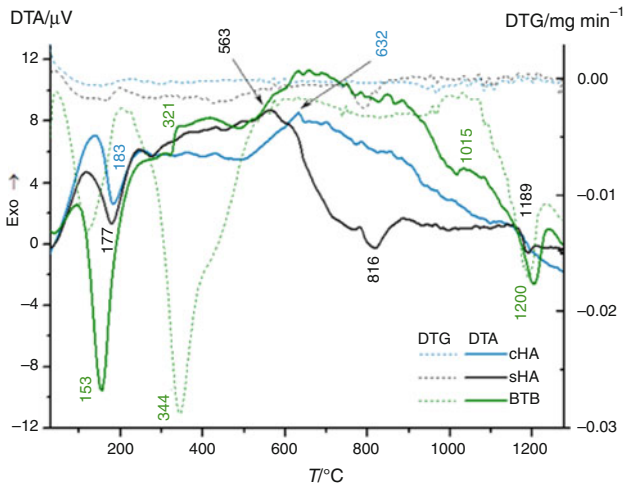

Fig. 3 DTA/DTG curves of the powdered samples cHA, sHA and biological sample BTB

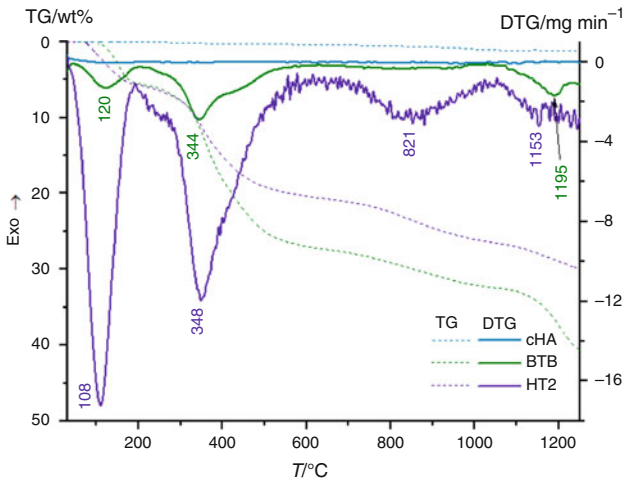

Fig. 4 TG/DTG curves of cHA, BTB and HT2

sHA and cHA

The crystalline structure acquired samples were determined through an XRD using RA. XRD analysis confirmed that sHA and cHA are monophasic and consist of HA with the space group $P6_3/m$ and with crystallite size ~30 nm, respectively ~80 nm.

The TGA/DTA analysis was performed for sHA and cHA samples in the form of powder from 25 to 1280 °C. The obtained TG and DTG curves for cHA are shown in Fig. 4. The sample cHA proved minimum weight loss in two steps with an endothermic process at 183 °C (0.2 wt%) and exothermic process at 632 °C (1 wt%), details are better shown in Fig. 3. The cHA transforms partly into hilgenstockite (HIL, $Ca_4P_2O_9$). The comparison of DTA/DTG curves for cHA and sHA is demonstrated in Fig. 3. The TGA/DTA results with temperature ranges of observed peaks and corresponding weight losses are for all samples summarised in Table 3 together with the analysis of escaped gases. After the TGA/DTA analysis and heating up to 1280 °C all the samples were analysed to detect constituent phases and structural parameters by using XRD, which are summarised in Table 4. The TG curve for sHA shows three regions of mass decrease (3). The first gradual weight loss with endothermic process (up to 220 °C) is due to liberation of the coordinated water molecule and partial decarboxylation. The second region of weight loss is due to fractional dehydration of lattice molecule water in temperature range 200–636 °C. Third region (~816 °C) is again caused by lost lattice water and decarboxylation. As it is already known, HA has two types of water in its structure: adsorbed and lattice water [27]. Adsorbed water is characterized by reversibility and thermal instability from 25 to 200 °C. Lattice water is lost reversibly at the temperature 200–400 °C.

The structural analysis of all samples confirmed that only the phase HA is presented. The structural parameters (a, c) of all the studied samples do not differ significantly from the values reported in the literature for CPs studies [1, 28]. The elemental analysis was done only for biological samples in different parts of their cross-sections as is illustrated in Fig. 2. On the BTB sample can be distinguished two areas A and B different in colour. The results of elemental analysis for both these areas summarised in Table 2 shows that there is, within the error limits, the same content of oxygen, phosphorus and calcium.

Table 4 The structural parameters and constituent phases of the obtained samples after thermal analysis

Sample	Phase	Formula	Space group	w/wt%	Unit-cell dimensions				Approximate crystallite size/nm
					a/Å	*b*/Å	*c*/Å	*β*/°	
cHA	HA	$Ca_{10}(PO_4)_6(OH)_2$	$P6_3/m$	91	9.4020	–	6.8869	–	151
	HIL	$Ca_4P_2O_9$	$P12_11$	9	7.0172	11.9797	9.4570	91.0	162
sHA	HA	$Ca_{10}(PO_4)_6(OH)_2$	$P6_3/m$	26	9.4148	–	6.8892	–	138
	TCP	$Ca_3(PO_4)_2$	$P12_1/a1$	74	12.8870	27.2800	15.2190	126.2	186
BTB	HA	$Ca_{10}(PO_4)_6(OH)_2$	$P6_3/m$	80	9.4510	–	6.8802	–	133
	Lime	CaO	Fm3m	14	4.8044	–	–	–	188
	HIL	$Ca_4P_2O_9$	$P12_11$	6	7.0107	11.9949	9.4656	90.8	118
HT1	WHI	$Ca_{2.86}Mg_{0.14}(PO_4)_2$	R3cH	98	10.3565	–	6.8850	–	90
	HA	$Ca_{10}(PO_4)_6(OH)_2$	$P6_3/m$	2	9.4142	–	6.8812	–	150
HT2	WHI	$Ca_{2.86}Mg_{0.14}(PO_4)_2$	R3cH	98	10.4109	–	37.4265	–	115
	HA	$Ca_{10}(PO_4)_6(OH)_2$	$P6_3/m$	2	9.4036	–	6.9181	–	183
HT3	WHI	$Ca_{2.86}Mg_{0.14}(PO_4)_2$	R3cH	98	10.3876	–	37.4018	–	83
	HA	$Ca_{10}(PO_4)_6(OH)_2$	$P6_3/m$	2	9.4268	–	6.8961	–	104
	HIL	$Ca_4P_2O_9$	$P2_1$	*t.a*	7.0139	11.9853	9.4636	90.8	133

HIL hilgenstockite, *WHI* whitlockite, *t.a.* trace amount

Moreover, the structure of bone contained trace amount of zinc which is the only compositional difference between areas A (0.78 at.%) and B (0.42 at.%).

Central incisor (HT1), first premolar (HT2) and second molar (HT3) suggest a relatively similar structure. They contain mainly oxygen, calcium, phosphorus and small unknown amounts of sodium, magnesium and aluminium. In addition, zones A and B (central part) in samples HT2 and HT3 indicates the trace amount of copper between 0.1 and 0.2 at.%. In the case of central incisor HT1 the amount of oxygen (Table 2) slightly decreases from the central part (zone A, B) to the outskirts of the sample (zone E) and the oxygen content is markedly lower for the periphery (zone F). As the oxygen content decreases amongst the zones A–E the content of phosphorus and calcium slightly increases with the high increase for periphery zone F. As is seen in Table 2 the ratio Ca/P content is practically the same for zones A–E, and is higher for periphery zone F. The amounts of magnesium and aluminium decrease from the centre to periphery, but the content of sodium increases. In the case of first premolar HT2 are the changes of ions content with the zones almost opposite to HT1 results. In addition, the HT2 sample microanalysis especially for zones A and B shows extreme values of concentration of some ions compared to results for other studied zones of sample HT2. Also the Ca/P ratio is low for zones A and B, but for other zones, the value of ratio is close to 1.5 which is comparable with the sample HT1. Similar extremes in ion content were obtained for second molar HT3 sample too, so that the only clear dependence factor for chemical element content is the decreasing amount of oxygen from the centre of the sample to periphery, and increasing content of magnesium is direction from zone A to C. The periphery zone F presents minimum of oxygen, sodium, magnesium and aluminium content and maximum of phosphorus.

The theoretical molar Ca/P ratio for stoichiometric HA should be equal to 1.67. However, it has already been described that the bone-apatite is characterized by calcium, phosphorus and hydroxyl deficiency where the molar Ca/P ratio varying from 1.37 to 1.87 [21]. The internal crystal disorder and ionic substitution within the apatite lattice results in the presence of significant levels of additional trace elements within bone mineral which play a role in overall performance of human bone [29–31]. Concerning the molar Ca/P ratio the periphery part (zone F) of sample HT1 and HT3 are close to stoichiometric HA. All other tested parts of bone and teeth samples have the molar Ca/P ratio within the published limits except centre (zone A and B) of sample HT2 and HT3 where the ratio is as low as 1.15 (only in these areas was detected small amount of copper).

The bone and teeth composition differs depending on site, age, dietary history and the presence of disease [32]. The studied teeth samples are not from comparable persons but generally the elemental analysis indicates two evidently different zones, central part and periphery (zones F for HT1, and HT2; and zone D from sample HT3) with lower amounts of oxygen and greater amounts of calcium and phosphorus. This contrast was confirmed by XRD as two structures, HA1 and HA2.

The thermal analysis data of sHA and cHA can be compared to the data for studied biological samples as well as XRD analysis results for all samples after thermal

treatment up to 1280 °C (Tables 3, 4). The sample cHA proves weight loss in two steps, but the sHA demonstrates three steps. The sHA dehydration does not occur instantly but over wide temperature range. In the temperature range of 1150–1210 °C, the peak of sHA could be connected with conversion into TCP (Table 4). The obtained cHA and sHA have lower crystalline size (Table 4) than that published for commercial HA from Table 1. The compositions of cHA and sHA after calcination up to 1280 °C were dissimilar, and it could be a consequence of other phase presence (well crystalline HIL and TCP). After the calcination, there is a huge difference in HA content between cHA (91 wt%) and sHA (26 wt%).

In the case of BTB sample, the weight loss occurs in three steps, and their temperature regions are close to that for sHA (Table 3). The last weight loss effect for BTB around 1015 °C is probably the transition of natural HA into HIL, the same as for cHA. Furthermore, the sample BTB undergoing calcinations up to 1280 °C contained lime (CaO) as a product of decomposition of organic matrix. The presence of HA and CaO after calcination up to 1280 °C is comparable with the published results for calcination of bone at 800 °C (Table 1) but, moreover, the higher temperature caused partial transformation of present HA phase into HIL.

The published analysis of enamel and dentin after calcination at 800 °C (Table 1) proved the presence of β-TCP and HA, but in our samples calcinated at 1280 °C, there is no TCP, but the major phase is whitlockite (98 wt%) with HA (2 wt%), and in the case of HT3 also showed trace amount of HIL. The results for teeth HT1 and HT2 after calcination correlate well which can arise from comparable molar Ca/P ratio (Table 2) before calcination. The tine HT3 has a bit lower molar Ca/P ratio and significantly lower weight loss in 196–571 °C temperature range, and after calcination HT3 contain small amount of HIL. On the other hand, BTB after calcination contains 6 wt% of HIL and has molar Ca/P ratio comparable with the HT,1 but compared to HT1 has higher weight loss up to temperature about 500 °C.

Conclusions

This study submits the structural and thermal properties of synthetic and biological samples containing HA. The combination XRD and SEM-EDX microanalysis affords more information about the samples and their composition. All samples of human teeth contained two types of HA with different crystalline size. The HA crystals of enamel are much larger as evidenced by the higher crystallinity demonstrated in their XRD patterns. The XRD patterns of enamel's HA showed narrower and sharper diffraction peaks compared to those in the XRD patterns of dentine or bone. The BTB sample was composed of HA as only one compact mineral phase. The molar rations Ca/P in biological samples were lower in comparison with molar ration of theoretical HA. The elementary analysis by EDX proved important divergence of molar ration Ca/P between the centre and periphery of the cross-sectional samples of teeth. Furthermore, zones A and B of cross-cut samples of HT2 and HT3 contained Cu and the sample BTB contained small amount of zinc. Thermal analysis showed several regions of dehydration and decomposition of the matrix. After calcination up to 1280 °C, the sample cHA contained predominantly HA (91 wt%) and remanent part as HIL, whereas the sample sHA included only 26 wt% HA and mainly TCP (74 wt%). In the case of BTB, thermal analysis indicated partly transformation into HIL too, and main component of transformation process was HA (80 wt%) and 14 wt% CaO. Teeth samples HT1–HT3 largely transformed into WHI, where HT1 and HT2 had obviously loss of weight then sample HT3 during the calcination to 600 °C. XRD results of the second molar (HT3) showed the trace amount of HIL after calcinations. In case of all samples, crystal growth of HA occurred during the thermal treatment. Mass spectroscopy of the undergoing gas of HT2 and HT3 identified the trace amounts of fragments with F^{+} and F^{2+}, which previously was not detected by XRD or EDX microanalysis.

Acknowledgements This study was supported by the Czech Ministry of Education, Youth and Sports under the project MSM 0021627501, and IGA University of Pardubice (SGFChT04). Special thanks to Milan Vlček from Joint Laboratory of Solid State Chemistry, University of Pardubice.

References

1. Palmer LC, Newcomb CJ, et al. Biomimetic systems for hydroxyapatite mineralization inspired by bone and enamel. Chem Rev. 2008;108:4754–83.
2. Dorozhkin SV. Calcium orthophosphates in nature, biology and medicine. Materials. 2009;2:399–498.
3. LeGeros RZ. Formation and transformation of calcium phosphates: relevance to vascular calcification. Z Kardiol. 2001;90:116–24.
4. Ito A, Onuma K. Crystal growth technology. London: Wiliam Andrew Publishing; 2003.
5. Chen ZF, Darvell BW, Leung VWH. Hydroxyapatite solubility in simple inorganic solutions. Arch Oral Biol. 2004;49:359–67.
6. Yujiro W, Toshiyuki I, Yasushi S. Type-A zeolites with hydroxyapatite surface layers formed by an ion exchange reaction. J Eur Ceram Soc. 2006;26:469–74.
7. Reddy MP, Venugopal A. Hydroxyapatite photocatalytic degradation of calmagite (an azo dye) in aqueous suspension. Appl Catal B. 2007;69:164–70.
8. Baillez S, Nzihou A, Bernache-Assolant D. Removal of aqueous lead ions by hydroxyapatites: equilibria and kinetic processes. J Hazard Mater. 2007;139:443–6.

9. Reddy MP, Venugopal A, Subrahmanyam M. Hydroxyapatite-supported Ag-TiO_2 as *Escherichia coli* disinfection photocatalyst. Water Res. 2007;41:379–86.
10. Omelon SJ, Grynpas MD. Relationships between polyphosphate chemistry, biochemistry and apatite biomineralization. Chem Rev. 2008;108:4694–715.
11. Rey C, et al. Chemical diversity of apatites. Adv Sci Technol. 2006;49:27–36.
12. Daculsi G, Bouler JM, LeGeros RZ. Adaptive crystal formation in normal and pathological calcifications in synthetic calcium phosphate and related biomaterials. Int Rev Cytol. 1997;172: 129–91.
13. LeGeros RZ. Calcium phosphates in oral biology and medicine. Basel: Karger; 1991.
14. Prakash KH, et al. Apparent solubility of hydroxyapatite in aqueous medium and its influence on the morphology of nanocrystallites with precipitation temperature. Langmuir. 2006;22: 11002–8.
15. Sanosh KP, et al. Preparation and characterization of nano-hydroxyapatite powder using sol–gel technique. Bull Mater Sci. 2009;32:465–70.
16. Yoon SY, et al. Synthesis of hydroxyapatite whiskers by hydrolysis of α-tricalcium phosphate using microwave heating. Mater Chem Phys. 2005;91:48–53.
17. Earl JS, et al. Hydrothermal synthesis of hydroxyapatite. J Phys Conf Ser. 2006;26:268–71.
18. Kaloustian J, et al. The use of thermal analysis in determination of some urinary calculi of calcium oxalate. J Therm Anal Calorim. 2002;70:959–73.
19. Madhurambal G, Subha R, Mojumdar SC. Crystallization and thermal characterization of calcium hydrogen phosphate dihydrate crystals. J Therm Anal Calorim. 2009;96:73–6.
20. Paulik F, et al. Investigation of the composition and crystal structure of bone salt by derivatography and infrared spectrophotometry. Hoppe Seyler's Z Physiol Chem. 1969;350:418–26.
21. Mezahi FZ, et al. Dissolution kinetic and structural behaviour of natural hydroxyapatite vs. thermal treatment. J Therm Anal Calorim. 2009;95:21–9.
22. Mitsionis AI, Vaimakis TC. A calorimetric study of the temperature effect on calcium phosphate precipitation. J Therm Anal Calorim. 2010;99:785–9.
23. Holager J. Thermogravimetric examination of enamel and dentin. J Dent Res. 1970;49:546–8.
24. JCPDS PDF-2 database, release 54. Newton Sq.: International Centre for Diffraction Data; 2004.
25. Diamanti I, et al. Effect of fluoride and of calcium sodium phosphosilicate toothpastes on pre-softened dentin demineralization and remineralization in vitro. J Dent. 2010;38:671–7.
26. Hattab FN. The state of fluorides in toothpastes. J Dent. 1989;17: 47–54.
27. LeGeros RY, Bonel G, Legros R. Types of H_2O in human enamel and in precipitated apatites. Calcif Tiss Res. 1987;26:111–8.
28. Wang L, Nancollas GH. Calcium orthophosphates: crystallization and dissolution. Chem Rew. 2008;108:4628–69.
29. McConnell D. Apatite. Vienna: Springer; 1973.
30. Posner AS. Crystal chemistry of bone mineral. Physiol Rev. 1969;49:760–92.
31. Shi D. Biomaterials and tissue engineering. Berlin: Springer; 2004.
32. Aras NK, Yiimaz G, Alkan S, Korkusuz F. Trace elements in human bone determined by neutron activation analysis. J Radioanal Nucl Chem. 1999;239:79–86.